NASA Technical Memorandum 88184

Airborne Astronomy Program
Medium Altitude Mission Branch
Preprint Series 038

Star Formation in the Inner Galaxy: A Far-Infrared and Radio Study of Two HII Regions

D.F. Lester, H.L. Dinerstein,
M.W. Werner, P.M. Harvey,
N.J. Evans II, and
R.L. Brown

December 1985

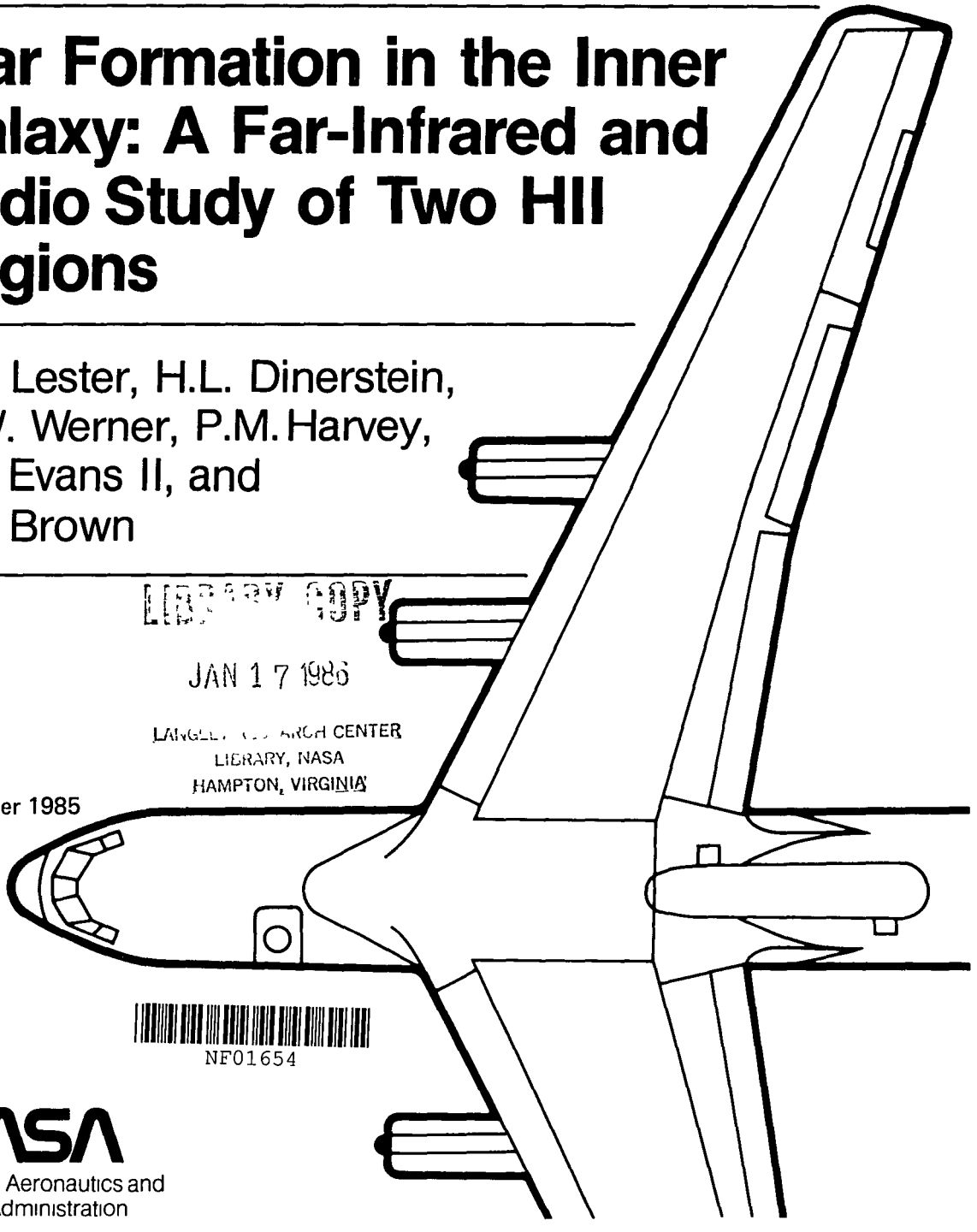

National Aeronautics and
Space Administration

NASA Technical Memorandum 88184

Airborne Astronomy Program
Medium Altitude Mission Branch
Preprint Series 038

Star Formation in the Inner Galaxy: A Far-Infrared and Radio Study of Two HII Regions

D. F. Lester,
H L. Dinerstein, University of Texas at Austin, Austin, Texas
M. W. Werner, Ames Research Center, Moffett Field, California
P. M. Harvey,
N. J. Evans II, University of Texas at Austin, Austin, Texas
R. L. Brown, National Radio Astronomy Observatory, Charlottesville, Virginia

December 1985

National Aeronautics and
Space Administration

Ames Research Center
Moffett Field, California 94035

This Page Intentionally Left Blank

I. INTRODUCTION

It now seems well established that the inner spiral arm region of our galaxy, at galactocentric radii from 4 to 6 kpc, is a region of greatly enhanced star formation. Surveys of CO emission (Scoville and Solomon 1975; Gordon and Burton 1976) indicate that the mean density of molecular cloud material may be nearly an order of magnitude higher there than in both the solar neighborhood and the region between this 5 kpc ring and the galactic center. Enhancements at 5 kpc are also seen in the distribution of HII regions (Lockman 1976), OH/IR stars (Baud, Habing and Oort 1979), pulsars (Taylor 1979), and cool giant stars (Ito, Matsumoto and Uyama 1977), all of which reflect enhanced star formation in the recent past. The conditions under which stars must form in this part of the Galaxy are unusual compared with solar neighborhood conditions. Not only is the mean density of radiation and matter much higher than in the solar neighborhood, but there is evidence that this region has been enriched in heavy elements relative to regions more distant from the galactic center, presumably because of the enhanced star formation rate (*c.f.* Mezger *et. al.* 1979, Lester *et. al.* 1985).

In view of the unusual conditions and the lack of detailed studies of star-forming regions in this part of the Galaxy, we undertook a study of two particularly bright HII region complexes, G30.8-0.0 and G25.4-0.2. We observed these regions photometrically at 40, 50, 100, and 175 μm with 50″ resolution and with considerably higher spatial resolution in the 6 cm continuum. Additional information about G25.4-0.2 was provided by measurements of the strength and distribution of [SIII] 9532Å as well as the velocity structure in H86α and CO. These data give us considerable insight into the structure and stellar population makeup of these inner galaxy HII regions which are, presumably, excited by very young OB stars. We compare these complexes with those at larger galactocentric distances which form the basis for the present general picture of massive star formation. Complementary infrared spectral data on these regions are discussed in separate papers (Lester *et. al.* 1983, 1985), in which it is shown that they may have high N/O abundance ratios.

II. OBSERVATIONS

The infrared measurements were made using a photometer and filter set similar to that described by Harvey (1979). The effective wavelengths of 40, 50, 100, and 175 μm are those applicable to sources with the observed color temperatures. Observations were made from the Kuiper Airborne Observatory 91 cm telescope using a bolometer system at the straight-Cassegrain focus. A 50″ (FWHM) beam was used, and the chopping secondary was operated with a beam spacing of 6′ at PA≈70° and 85° for G30.8-0.0 and G25.4-0.2 respectively. Maps in the 50 and 100 μm filters were made by measuring the two wavelengths simultaneously at each point on the sky, which simplifies the derivation of color temperature. Measurements in all four filters were made at the main peaks in the two regions. The absolute positional accuracy of the maps is estimated to be about 10-15″. The signal at each position and in each filter was corrected for residual water vapor using extinction coefficients of 0.01, 0.02 , 0.03, and 0.02 per micron of precipitable H_2O at 40, 50, 100, and 175 μm respectively. During the observations of each source, the water column density varied between 10 and 15 μm.

The far-infrared maps were made by scanning the telescope in azimuth (along the direction of the chop) at a range of elevations in increments of 40″ in both axes. The azimuth scans were approximately 7′ long and covered a range of approximately 9′. Each azimuth scan was deconvolved to remove the effects of spatial chopping under the assumption that the average of the signal at the two endpoints of the scan defined zero flux. After this procedure was applied, the lowest dependable contours were 100 and 300 Jy-beam^{-1} at 50 and 100 μm respectively. The 50/100 μm color temperature was derived by taking the ratio of the 50 and 100 μm fluxes at each position and by determining the corresponding color temperature. Since the color temperatures will have substantial uncertainties at low flux levels, only the values at positions with substantial flux are presented below.

Flux density calibration was accomplished by observing S140, which was assumed to have 4600, 5700, 6000, and 4200 Jy at 40, 50, 100 and 175 μm respectively (Harvey, Campbell and

Hoffman 1977; see also their note added in proof). The accuracy of the flux density is, except for the lowest contour in each map, limited by the absolute calibration and water vapor measurements to approximately 30%, as the signal-to-noise was high at most positions. The far-infrared spectral distributions at the peak positions in G30.8 and G25.4 were derived, and total flux densities at 50 and 100 μm were determined by integrating the maps.

Measurements of the 9532Å [SIII] line in G25.4 were made using a sequential scanner with a 4Å bandpass on the Crossley telescope at the Lick Observatory. A Varian VPM-164 photomultiplier was used for these observations. Measurements were made with a 30″ aperture and are referenced to the sky approximately 10′ away. The fact that the source is not seen on the Palomar Sky Survey red print implies that there is substantial visual extinction. Near the peak of the emission in G25.4-0.2 the line is the bright enough that the calibration procedure is the dominant source of error, which is estimated to be about 20%. The instrument is further described by Hawley and Grandi (1977). The absolute positions on this [SIII] map are accurate to about 10″. Although only the region around the SE component of G25.4-0.2 was mapped, no emission was detected in a single beam position at the NW peak of that complex.

The radio continuum maps were made at 4866 MHz with the VLA.[5] A concatenation of

---

[5]Operated by Associated Universities Inc., under contract with the National Science Foundation.

---

snapshot (u,v)-data was made from observations taken at separate epochs in the two short configurations, the C- and D-arrays. This provides a continuous distribution of projected baselines from 40 to 1800 m and resultant synthesized Gaussian beams of 9.2x6.8" at PA≈ 52° and 7.4x6.5" at PA≈ 56° for G30.8 and G25.4 respectively. The flux density calibration was referred to 3C286; we adopted 7.41 Jy for this source at our observing frequency. The bandwidth used for these observations, 12.5 MHz, was sufficiently narrow that we could map the entire primary telescope beam and thus obtain a CLEAN map free from effects due to confusing sources of

galactic emission anywhere in the beam. For G25.4, the total flux in the map is 6.1 Jy (3.5 and 2.6 Jy from SE and NW respectively). This is somewhat smaller than the 19.1 Jy found by Downes *et. al.* (1980), leading us to believe that our VLA map is not sampling some extended emission in the vicinity. Especially short baselines were used in the concatenation for G30.8 and, as a result, very little extended emission is likely to be missed for that source. The total flux density in our G30.8 map is 57.4 Jy, which agrees well with the single dish results. The total flux densities for the separate components of G30.8 are thus listed in Table 1.

In order to obtain the velocity of the ionized gas associated with the two separate components G25.4SE and G25.4NW, we observed the H89α 9.173 GHz radio recombination line from both of these objects. These observations were made with the Cassegrain upconverter-maser receiver on the NRAO 140-foot telescope.[5] The system temperature on cold sky was 42°K. A single 1024-channel spectrum covering 20 MHz bandwidth was produced in the autocorrelation spectrometer; the velocity resolution was 0.6 km-s^{-1}. The telescope beamwidth at the line frequency, 3.′1 (FWHM) as determined from observations of Virgo A, was sufficiently small to allow us to distinguish the line emission from the two peaks of G25.4 seen in the far-infrared and VLA maps. We obtained spectra at both VLA positions. In order to verify that we were indeed pointed at the proper positions, immediately prior to the spectral line observations we established the telescope pointing using 1730-130 (NRAO 530). Following the spectroscopy at each position, we again observed 1730-130 and confirmed that the pointing was accurate and stable to within 5′′. These single dish measurements, which cleanly separate the two sources, provide the best continuum flux densities for them, and these are given in Table 1.

The G25.4 region was mapped in the 2-1 transition of ^{13}CO using the 4.9m antenna of the Millimeter Wave Observatory of the University of Texas[6]. An area of about

---

[6]The Millimeter Wave Observatory is operated by the Electrical Engineering Research Laboratory of the University of Texas at Austin., with partial support from the National Science Foundation and McDonald Observatory.

6x10′ centered on the far-infrared and radio continuum sources was surveyed , using a beam spacing of 1', which is smaller than the 1.3' FWHM beam. The velocity resolution was 0.33 km-s^{-1}, and data were taken in 256 velocity channels. Thus the main components at 65 and 95 km-s^{-1} were mapped simultaneously. The system noise temperature was typically 1400°K. The absolute position reference was checked by scans of Jupiter and Saturn, and is estimated to be accurate to about 15′′.

III. MORPHOLOGY AND INFRARED LUMINOSITY

a) G30.8-0.0 (W43)

The galactocentric distance of 5.4 kpc adopted for this source is based on the +90 km-s^{-1} component of H110α. Recombination line spectra taken around the region covered by our 6x6′ maps show that this velocity component is by far the dominant one over this restricted area (Gardner and Thomasson 1975). The distance ambiguity is resolved by lack of H_2CO absorption at velocities larger than this (Downes *et. al.* 1980), and a heliocentric distance of 7 kpc is indicated.

Pipher, Grasdalen and Soifer (1974) mapped the region at 12 μm and found the hot dust to be distributed similarly to the 5 GHz emission which they synthesis-mapped with very limited baseline coverage. The single-dish radio map that best matches the far-infrared beam is the 23 GHz map at 80′′ resolution by Rodríguez and Chaisson (1978). At 100 μm, five peaks are distinguishable in the infrared maps. The far-infrared positions and fluxes for these sources are given in Table 1. The brightest two sources, which we will designate G30.8N and G30.8S, correspond to the main radio and 12μm peaks.

Our VLA map allows the comparison of radio structure to infrared structure to be made in detail. Comparing the infrared maps of G30.8 (Figures 1a, b, c) with the VLA map (Figure 2), it is seen that four of the five far-IR sources are also radio continuum sources. The westernmost source in the VLA map, corresponding to infrared source #4, resembles a thin rim seen edge-on. This morphology is shared by source #3 to the northeast, and, to some extent, by G30.8N (source #1) at top center. Infrared source #5 is associated with extended low-surface-brightness nebulosity. The 0.2 Jy compact radio source seen near that position (at $18^h\ 45^m\ 05.^s7$ -02° 03' 43") is unresolved, and may not be associated with the W43 complex. The general agreement between the far-infrared and radio recombination emission indicates that absorption of photons

from the hot stars which ionize the H II region is responsible for heating the dust radiating in the far-infrared.

Comparison of the 50 and 100 μm maps reveals an overall similarity, but noticable differences in detail. For example, the position of peak flux in G30.0S is significantly different in the two maps; the 50 μm peak of this source is displaced to the north relative to its 100 μm position. Furthermore, the peripheral peaks #3 and #5 are much stronger at 100 μm than at 50 μm, as compared with G30.8N and G30.8S. This effect shows up well on the color temperature map, in which G30.8N and G30.8S have peak color temperatures of ≈65°K while sources #3 and #5 have color temperatures of ≈45°K, which is unusually cool compared with other HII regions (Harvey, Campbell and Hoffman 1977; Thronson and Harper 1979). A recent map of H_2CO absorption across G30.8 (Beiging *et. al.* 1982) offers one explanation for this situation. This map was used to construct the map of H_2CO equivalent width that is shown in Figure 1d. Although the H_2CO beam is three times larger than that for the infrared measurements, it is clear that there is considerable structure in the molecular gas within the boundaries of our far-infrared map, with the largest absorptions toward sources #3 and #5. Using the relation of Federman and Evans (1981), $A_V \approx 12W(H_2CO)$, we expect several hundred magnitudes of visual extinction along the line of sight to at least parts of these sources. Assuming a λ^{-1} extinction law beyond 10 μm, this corresponds to several extinction optical depths around 100 μm and a differential extinction of order unity between 50 and 100 μm. We note that this molecular gas along the line of sight need only be colder than the emitting dust in the HII region in order that flux be removed from the beam. This extinction could account for the faintness of these sources at 50 μm.

The far-infrared sources along the northern border of G30.8 (sources #3, #1=N, and #4) might be interpreted as ionization fronts along neighboring molecular clouds, an interpretation supported by their ridgelike structure at 6 cm. Even the lowest contour of the H_2CO absorption map predicts a rather large extinction in the near-infrared , so the visibility of the complex at 12μm and, indeed, at shorter wavelengths (see below) would suggest that the molecular gas is clumped on a scale considerably smaller than the 2.′5 H_2CO beam.

It can be seen from the spectra of G30.8N and G30.8S and the integrated spectrum for the entire complex (see Figure 3) that the extended emission around G30.8 is cooler than that from the core. This is also evident from the color temperature map in Figure 1c. This result is not unexpected in view of the extinction at the periphery of the nebula. Using a mean 50/100 μm color temperature of 51°K for the entire mapped region, we derive F_{total}= 2.2 x 10^{-9} W-m^{-2} for the total integrated far-infrared flux of the mapped region, assuming a blackbody spectral distribution as indicated in Figure 3. The contribution of the short wavelength wing of the spectral distribution (which is especially evident in the spectra at the peaks) to the total flux is negligible because the wing does not share the spatial extent of the 100 μm emission. At the assumed distance of 7 kpc, the integrated flux corresponds to a luminosity of 3.3 x 10^6 $L_\odot$. Within one beamsize (a projected diameter of 1.7 pc at the distance of G30.8), the luminosities of G30.8N and G30.8S are similar, about 2 x 10^5 $L_\odot$ for each source.

The fact that the dust color temperature peaks near the center of the complex indicates that a discrete luminosity source is in the vicinity. The peak of the color temperature is, interestingly, not coincident with either G30.8N and G30.8S, but lies in between them. Concentrations of 6 cm emission are seen not only at the two main far infrared peaks, but also between them, where the infrared contours show a saddle minimum. This region was observed with the NASA IRTF to look for a near-IR counterpart to this source. A bright source was detected at this peak, with K=8.3 at (1950) 18^h 45^m $00.^s0$ -01° 59′ 54″ ±2″. In a 6″ circular aperture, this source appeared unresolved. Although a complete survey of the region was not made, and measurements at other wavelengths were not obtained, it seems plausible that this near-infrared source is the dominant luminosity source for the core of G30.8. Morphologically, this source is near the center of symmetry of the rim sources discussed above. The VLA map shows a local maximum at the position of this near infrared source. Assuming that this source is a hot star, K=8.3 corresponds to a main sequence star of 5 x 10^5 $L_\odot$ in the absence of any 2μm extinction. In order to supply the observed total luminosity of 3.3 x 10^6 $L_\odot$, we need to invoke an extinction of two magnitudes, or $A_V \approx 20^m$, which is not unreasonable. A more complete understanding of the role of this near-

infrared source will have to await a more thorough survey of the region. It will also be necessary to consider the possibility that the 2μm emission may be seriously contaminated with dust or gas emission.

b) G25.4-0.2

Our infrared map for this source (Figure 4) clearly distinguishes two components, which we will designate as G25.4SE and G25.4NW. We note that G25.4NW is somewhat more extended in the far-infrared than is G25.4SE, and that the blackbody color temperature at the peak of G25.4NW (59°K) is substantially lower than that for G25.4SE (80°K). These two components are also seen in the VLA map of the complex (Figure 5). These two radio components have also been detected, though with much more limited uv-plane coverage, by Felli, Tofani, and D'Addario (1974) and Krassner *et. al.* (1983). The 15 GHz single-dish map of Schraml and Mezger (1969) shows the source to have a pronounced asymmetry, which we now understand in terms of its duplicity.

There has been considerable uncertainty about the distance to the G25.4-0.2 complex. The brightest component of H109α in this direction is at 59 km-s^{-1}, which corresponds to a galactocentric distance of 6.2 kpc (Churchwell *et. al.* 1978). Absorption near the tangent point velocity is seen in H_2CO (Wilson 1972; Downes *et. al.* 1980) and OH (Turner 1979), which would ordinarily imply the far kinematic distance of, in this case, 13.5 kpc. This value can be questioned, however. Comparing the measured 9532Å [SIII] surface brightness of G25.4SE (Figure 6) with the radio continuum surface brightness, as estimated by the flux in a similar beam from our VLA data, and making the reasonable assumption that most of the sulfur in the nebula is doubly ionized, we require 4.7 magnitudes of extinction at 9532Å, which corresponds to about 11 magnitudes of visual extinction. If G25.4SE were at a distance of 13.5 kpc, such a small extinction, for a source seen directly through the galactic disk, would be very surprising. We note parenthetically that, to our knowledge, this is the first map of a heavily obscured HII region in the 9532Å line. It should be noted that this line will dominate I-band photometry of HII regions and, in the case of intrinsic silicon detectors, which exclude HeI 10830Å, will dominate the nebular flux at wavelengths longer than Hα.

There are several possible explanations that might be invoked to overcome this problem. One possibility, that of a low extinction "tunnel" through the galactic plane, seems rather far-fetched. Downes *et. al.* (1980) noted that the apparent constancy of H_2CO line depth with beamsize suggested that this source was unusual, and first suggested the possibility of beam contamination by other sources at different distances along the line of sight. Our CO and small-beam recombination line measurements have verified this suggestion, with the surprising twist that it is G25.4SE and G25.4NW themselves that lie at very different distances, and that chance superposition accounts for their apparent proximity. Figure 7 shows the H86α profiles in the direction of these two components. Since the two components are separated by 2.′6 , we can obtain a line measurement from each of them separately, and expect only slight contamination from the other in the skirt of the 3.′15 FWHM beam of the 140-foot telescope. It is easily seen that the recombination line velocities differ greatly for the two components. G25.4SE, whose spectrum is shown at the top of Figure 7, has the stronger line of the two, with V_{LSR}= +59.1 km-s^{-1}. This is the component that dominated the earlier, large-beam, emission line velocities. G25.4NW, whose spectrum is shown at the bottom of Figure 7, has V_{LSR}= +99.0 km-s^{-1}; its spectrum is slightly contaminated on the low velocity side by the stronger line of its apparent neighbor. Both lines are also visible in an H103å spectrum centered on G25.4SE in a 5.1' beam. The +99.0 km-s^{-1} component was actually detected in the earlier work on this source by Churchwell *et. al.*, but was inconspicuous in their 2.6' beam which was centered on G25.4SE. It seems likely that it is G25.4NW against which the tangent-point H_2CO absorption is seen in the large-beam studies, an interpretation that can be directly checked when H_2CO absorption maps are made of this complex with a small beam. Barring an extraordinary dynamical situation, a picture thus emerges in which G25.4SE is at the near distance of 4.6 kpc, while G25.4NW is just beyond the tangent point, at a distance of about 12 kpc, and their apparent proximity is a projection effect. In view of the much larger distance to G25.4NW and the fact that its emission measure is similar to that of G25.4SE, the difference in 9532Å flux between the two sources is understandable as an extinction difference.

Our CO measurements add further to our understanding of this region. Figure 8 shows the MWO maps of ^{13}CO (2-1) in the two strongest components, which correspond approximately to the dominant radio recombination line velocities. Shaver *et. al.* (1982) and Leisawitz and Bash (1984) find evidence in several HII regions for velocities which are anomalous with respect to their galactic position, though the differences are generally an order of magnitude smaller than the velocity difference between G25.4NW and G25.4SE. On the other hand, the difference between the ionized gas velocity of +59 km-s^{-1} and the strong CO component at +65 km-s^{-1} for G25.4SE is not unusual. Israel (1978) has shown that such velocity differences between compact HII regions and their associated molecular clouds are common, and seen in many less obscured HII regions. The less obscured regions are presumably on the near sides of their molecular clouds, and the ionized gas is seen boiling off the cloud surface at thermal velocities.

It is clear from the CO map that the velocity structure of the molecular gas is also complicated in this region, with the 95 km-s^{-1} cloud lying farther to the west than the 65 km-s^{-1} cloud. This offset is in the same direction as that seen in the H86α data. Although the compact HII regions are not at the centers of their associated molecular clouds, it can be seen from this map that the G25.4 region has two distinct, high-column-density, molecular clouds at very different velocities that are superimposed.

The small-scale near infrared structure was investigated with the IRTF using a broadband 10 μm filter, 6″ aperture, and 30″ chopper throw. We find a 6″ diameter (FWHM) source at the center of G25.4SE with an unresolved core. The peak position of this source is (1950) $18^h\ 35^m\ 33.^s6$ -6° 50' 31" ±2", which is coincident with the radio, far-infrared and [SIII] peaks. The flux of this source is 10 Jy at 10 μm. This compares with values of 55 Jy in an 18″ beam measured by Zeilik (private communication), and 130 Jy from the AFGL survey. Therefore, a large part of the 10 μm emission from G25.4SE is in an extended envelope. A southern extension to the peak can be fit with a second source with one-third the flux of the main peak at a distance of 6". The near infrared structure of G25.4SE is thus very similar to that seen at 6 cm in our VLA map.

The spectral energy distribution for G25.4-0.2 and the two peaks is shown in Figure 9. We find that the color temperature peaks at the position of each component, as it must for separate luminosity sources. Assuming an average 50/100 μm color temperature of 65°K for the entire mapped region, and using the integrated fluxes at those wavelengths, we derive $F_{total} = 1.4 \times 10^{-9}$ W-m^{-2}. Slightly more than half of this flux lies within a 3′ radius of G25.4SE. Like the peaks in G30.8-0.0, these sources are optically thin in emission when the flux is averaged over the far-infrared beam, with $\tau < 0.01$ at 100 μm. It can be seen from Figures 1c and 4c that G25.4SE is hotter than G25.4NW and all of the sources in G30.8-0.0. Since G25.4SE is also the closest of all of these sources, the higher color temperature within our fixed-angular-size beam may result simply from sampling the hottest dust, if all of the sources have a common structure with temperature gradients decreasing outward from the sources of excitation.

G25.4SE may be ionized and heated by a single star, since the dominant core component is unresolved at a projected size of 0.1 pc at 4.6 kpc. At this distance, the source has a luminosity of 4×10^5 $L_\odot$, which is consistent with a single hot, main-sequence star. G25.4NW is seen from the VLA map to have a double structure, with the second peak lying 15″ farther toward the NW. This structure may at least partly account for the somewhat extended appearance of G25.4NW in the far-infrared maps. Although it is somewhat fainter than G25.4SE at all wavelengths, the large inferred distance (12 kpc) gives it a luminosity of 2.5×10^6 $L_\odot$, much higher than that of G25.4SE.

IV. COMPARISON OF INFRARED WITH IONIZING LUMINOSITY

Most of the short-wavelength ($\lambda < 20\ \mu m$) emission from hot dust in galactic HII regions can be accounted for by the absorption of resonantly trapped Lyα photons within the nebulae (see Wynn-Williams and Becklin 1974). In an ionization bounded HII region, each original Lyman continuum photon from the ionizing star is degraded by successive ionization and recombination. This results in a single Lyα photon that is eventually absorbed by a dust grain, plus some number of higher order recombination lines that escape the nebula with negligible cooling effect.

When the far-infrared emission ($\lambda > 20\mu m$) is included in the total luminosity of a typical giant HII region, Lyα heating is found to be insufficient to account for the thermal radiation from the dust. It seems likely that the additional heating is due to the absorption of stellar photons with $\lambda > 912$Å by dust in the adjacent cloud material just outside the Stromgren sphere. This interpretation is supported by detailed studies of regions like M17 (Gatley *et. al.* 1979) and G333.6-0.2 (Hyland *et. al.* 1980), which are likely to represent typical HII region - molecular cloud interfaces. The relationship between ionizing flux and infrared emission can be probed directly by using the thermal brehmsstrahlung emission at radio wavelengths as a gauge of ionizing photon flux. Except for unusually dense and dusty compact HII regions in which a signficant fraction of the Lyman continuum photons are absorbed directly by the dust before they are able to ionize hydrogen, it is usually assumed that the ratio of optically thin radio flux to integrated infrared flux is a measure of the ratio of ionizing to total flux from the exciting stars, and thus of the spectral character of those stars (Mezger 1978; Mezger and Smith 1975) . Following Emerson and Jennings (1978), we define an infrared excess for an HII region as $IRE = L_{IR}/N_c' h\nu_\alpha$, where L_{IR} is the total luminosity of the HII region, N_c' is the number of Lyman continuum photons produced by recombination in the gas, and $h\nu_\alpha$ is the energy of a Lyα photon. Rubin (1968) gives the number of stellar Lyman continuum photons absorbed by the gas as a function of free-free radio luminosity for an ionization bounded nebula. Since one Lyα photon is produced for a single Lyman continuum photon, we thus derive

$$IRE = 1.538 \times 10^{9} \, (F_{IR} / S_{\nu}) \, \nu^{-0.1} \, T_e^{0.45} \qquad (1)$$

where F_{IR} is the total flux from the region in W-m^{-2}, S_ν is the optically thin radio flux in Jy, ν is the radio frequency in GHz, and T_e is the electron temperature of the gas in °K.

The radio flux with which the infrared flux is to be compared must be measured over the same region as the infrared map. Furthermore, since the infrared intensity is assumed to be zero below the lowest contour on the maps in Figures 1 and 4, the radio brightness temperatures must be treated analogously. The single-dish maps are probably the most appropriate to use to derive total radio fluxes. The 23 GHz map of G30.8-0.0 by Rodriguez and Chaisson (1978) is already well matched in spatial resolution to our far-infrared map, and gives a total flux of 46±7 Jy. Our assumption that the emission at this frequency is optically thin is justified by the similarity of this value to the 5 GHz integrated flux from the VLA map (57 Jy). We thus derive for G30.8-0.0 an IRE of 2.4 to 3.3, corresponding to an assumed electron temperature in the range 5000 to 10000K. This is consistent with the value derived by Emerson and Jennings (1978).

For G25.4, the Schraml and Mezger (1969) map is the best match to the infrared map. In this case, since there is less extended emission than in G30.8, the boundaries of the far-infrared map and that of the 15 GHz map are similar. From their total 15 GHz flux of 19.7 Jy, we find that 18.7 Jy is within our mapped area. For assumed electron temperatures of 5000 and 10000K, we derive for G25.4 an IRE of 4.1 and 5.5 respectively.

The derived IRE values for G25.4 and G30.8 are very similar to the infrared excesses of outer-arm HII regions that have been measured in the same way (Harvey, Campbell and Hoffman 1977; Thronson and Harper 1979). This result constrasts sharply with a recent study by Boissé *et al.* (1981). These authors have compared the infrared surface brightness along the galactic plane measured with a wide-beam balloon-borne experiment with the radio continuum brightness temperature taken from the maps of Altenhoff *et. al.* (1970). Their comparison is made for measurements integrated into one degree bins of galactic longitude. They find a strong correlation

of IRE with galactic longitude (and therefore , presumably, with galactocentric distance) such that a representative IRE for an HII region complex in the 5 kpc ring is almost an order of magnitude higher than for complexes near the solar circle. Boissé *et. al.* find that in the region l=30 to 31°, a region dominated by W43, the IRE is 26 compared with our value of about 3.

The Boissé *et. al.* measurement assumed a constant ratio of integrated luminosity to luminosity within their long-wavelength passband. This requires that the color temperature not vary. As a result, it is worthwhile to check this claim of a high IRE with the more completely spectrally sampled data of Low *et. al.* (1977) and Nishimura, Low and Kurtz (1980), though their integrated beamsize of 30' is considerably smaller. Taking $F_{5\ GHz} = 90$ Jy for this beam and their derived 60-300 μm luminosity of 6×10^{-9} W-m^{-2} , one derives an IRE in the range 4- 6 which is only slightly larger than we derive in a 6′ area. We can investigate this difference further by comparing infrared fluxes for W43 taken in different apertures. Figure 10 shows the measured 100 μm flux as a function of beam area A. The point corresponding to the smallest aperture is from our study, in which the 6′ chopper throw defines the spatial limit of sensitivity. The results of Hoffman, Frederick and Emery (1971) , Low *et. al.* (1977) and Olthof (1974) with beamsizes of 12, 15, and 30′ respectively, are also shown. The integrated flux in a 60x22′ area is from Boissé *et. al.* The resulting curve shows that, from equivalent beam diameters of 6' to 30′, the 100 μm flux from W43 increases as $A^{0.35}$, implying a surface brightness varying as $r^{-1.35}$. For diameters larger than 30', however, the Boissé *et. al.* point suggests that the 100 μm flux varies even more rapidly than A. This would indicate a dominant contribution of emission on a scale of order 1° that does not correspond to ionized gas. The fact that this large-beam result is actually larger than an extrapolation assuming constant surface-brightness is difficult to understand, however, and may indicate an error in the Boissé *et. al.* analysis, perhaps in their conversion to integrated flux.

We point out that a variation of IRE with beamsize is not unexpected, however. Such an effect can be predicted for a single OB association in which subgroups of rather different ages are being sampled by different beamsizes. Ho and Haschik (1981) have investigated the IRE that might be

expected from a typical initial mass function with different upper and lower mass limits, using the data in Panagia (1973).[7]

---

[7]Avedisova (1979) has redone the calculations of Panagia (1973) with non-LTE model atmospheres. The agreement with the earlier result is excellent, especially for the O stars. For the purpose of this study, the Miller and Scalo (1979) IMF that was used by Ho and Haschik is not significantly different than that more recently derived by Garmany, Conti, and Chiosi (1982)

Using their results, we find that an IRE of 2.6 will be produced by an ensemble of stars with normal IMF and maximum mass of $\approx 50 M_{\odot}$, while an IRE of 26 corresponds to a population with a maximum mass of $22 M_{\odot}$. A $22 M_{\odot}$ star has a main sequence lifetime of $\approx 8 \times 10^6$ years (Chiosi, Nasi, and Sreenivasan 1978). If we assume that the original subgroup that dominates the large scale emission from l=30° had a velocity dispersion of 20 km-s^{-1}, which is the turbulent velocity now seen in the core of W43 (Turner *et. al.* 1974), a subgroup with the most massive star still on the main sequence having about $22 M_{\odot}$ would have expanded to approximately 160 pc by this time. This is exactly the projected beamsize (1°) of the Boissé *et. al.* study at the distance (7 kpc) of W43. Such a velocity dispersion for the stars in an association is also justifiable on the basis of observations of young OB associations in the field (Blaauw 1964).

V. SUMMARY

We have made far-infrared measurements of two inner-galaxy HII region complexes, G30.8-0.0 and G25.4-0.2. Measurements of the prominent peaks were made at 40, 50, 100, and 175μm, and the regions were mapped over an area of 15′ at 50′′ resolution, at 50 and 100μm. These observations have been combined with high resolution radio continuum maps and, for G25.4, radio recombination line and CO line measurements to better understand these regions, and to compare their properties with those of star-forming regions nearer to the solar circle. We summarize our findings as follows:

1) The far-infrared emission from each region is dominated by two sources. For both G25.4 and G30.8, the distribution of the far-infrared emission is similar to that of the radio emission, indicating that OB stars provide most of the heating.

2) There is evidence that extinction plays an important role in G30.8, even in the far-infrared.

3) A near-infrared point source has been detected in G30.8 at the position of peak far-infrared color temperature. This source, which is in between the two main far-infrared components, may be the ionizing star for the core of G30.8.

4) Our measurement of [SIII] 9532Å from G25.4SE indicates that the extinction toward this source is very low ($A_V < 10^m$). This low extinction is difficult to reconcile with previously determined distance measurements to this source. Our new observations show that the two components of G25.4 are probably at very different distances, and are seen coincidentally superimposed. Previous large-beam distance determinations for this source were confused by this

coincidence. G25.4SE is probably at the near distance of only 4 3 kpc, which allows the relatively small extinction to be more easily understood, while G25.4NW is about 12 kpc away.

5) Total luminosities of $3x10^6$ $L_\odot$ and $4x10^5$ $L_\odot$ are found for G30.8-0.0 and G25.4-0.2 SE respectively. Even though it appears slightly fainter than G25.4SE, G25.4NW is actually much more luminous because of its much larger distance, and is probably more like G30 8 in its total luminosity. Comparisons with radio continuum fluxes give infrared excesses of between 3 and 5. These luminosities and infrared excesses are simular to those found for bright,well-studied HII regions in the solar circle, when the same projected area is considered. Far-infrared photometric measurements of these regions need not require an anomalous IMF at 5 kpc from the Galactic center.

We thank the staff and crew of the Kuiper Airborne Observatory for their expertise in the execution of this project, and Bruce Wilking and Marshall Joy for assistance with the observations. This work was supported in part by NASA Grant 05-003-511 to the University of Hawaii and NSF Grant AST-8312332 to the University of Texas. The airborne observations were made while D.F.L. and H.L.D. held NRC Associateships at the NASA Ames Research Center. H.L.D. was partially supported by NASA-U. Texas Research Interchange NCA2-OR781-201 and by the Robert A. Welch Foundation.

TABLE 1

Positions and Fluxes

Source	100μm Peak R.A. (1950)	Dec.	F_{peak} (100μm)(Radio) (Jy in 50″ beam)		$\int F\, d\Omega$ (100μm)(Radio) (Jy)	
G30.8-0.0 (W43N)				(5 GHz)		(5 GHz)
(1) G30.8N	$18^h\ 45^m\ 00.0^s$	-1° 58′ 40″	2010	5.9	11000	16.2
(2) G30.8S	18 45 02.9	-2 01 00	2040	6.8	15700	15.6
(3)	18 45 09.1	-1 57 50	900	---	3680	13.8
(4)	18 44 47.6	-2 00 00	600	---	6600	9.4
(5)	18 45 00.9	-2 04 20	1200	---	6100	2.4
TOTAL					43080	57.4
Near-IR point-source	18 45 00.2	-1 59 54		[K = 8.3	<2″ at 2μm]	
G25.4-0.2						(10 GHz)
(1) G25.4SE	18 35 32.8	-6 50 35	3230	---	10700	12.2
(2) G25.4NW	18 35 25.0	-6 48 25	2630	---	6240	5.8
TOTAL					16940	18.0

REFERENCES*

Altenhoff, W. J., Downes, D., Goad, L. Maxwell, A., and Rinehart, R. 1970, *Astr. Ap Suppl* ,1, 319.

Avedisova, V. S. 1979, *Astr. Zh.*, 19, 965.

Baud, B., Habing, H.J., and Oort, J. H. 1979, in *IAU Symposium 84, The Large-Scale Characteristics of the Galaxy*, ed. W. B. Burton (Dordrecht: Reidel), p. 29.

Bieging, J. H., Wilson, T. L., and Downes, D. 1982, *Astr. Ap. Suppl.*, 49, 607.

Blaauw, A. 1964, *Ann. Rev. Astr. Ap.*, 2, 213.

Boissé, P., Gispert, R., Caron, N. Wijnbergen, J. J., Serra, G.,Ryter, C., and Puget, J. L. 1981,*Astr. Ap* , 94, 265.

Chiosi, C., Nasi, E. and Sreenivasan, S. R. 1978, *Astr. Ap.*, 63, 103.

Churchwell, E., Smith, L.F., Mathis, J., Mezger, P.G., and Huchtmeier, W. 1978, *Astr. Ap.*, 70, 719.

Downes, D., Wilson, T. L., Beiging, J., and Wink, J. 1980, *Astr. Ap. Suppl* , 40, 379.

Emerson, J. P., and Jennings, R. E. 1978, *Astr. Ap.*, 69, 129.

Federman, S. and Evans, N. J. 1981 *Ap. J.*, 248, 113.

Felli, M., Tofani, G. and D'Addario, L. R. 1974, *Astr. Ap.*, 31, 431.

Gardner, C. D., and Thomasson, P. 1975, *Astr. Ap.*, 45, 1.

Garmany, C. D., Conti, P. S., and Chiosi, C. 1982, *Ap. J.*, 263, 777.

Gatley, I., Becklin, E. E., Sellgren, K., and Werner, M. W. 1979, *Ap. J.*, 233, 575.

Gordon, M. A., and Burton, W. B. 1976, *Ap. J.*, 208, 346.

Harvey, P. M. 1979, *Pub. A.S P.*, 91, 143.

Harvey, P. M., Campbell, M. F. and Hoffman, W. F. 1977, *Ap. J.*, 211, 786.

Hawley, S. A., and Grandi, S. A. 1977, *Ap. J.*, 217, 420.

Ho, P. T. P., and Haschik, A. D. 1981, *Ap. J.*, 248, 622.

Hoffman, W. J., Frederick, C. L. and Emery, R. J. 1971, *Ap. J. (Letters)*, 170, L89.

Hyland, A. R., McGregor, P. J., Robinson, G., Thomas, J. A., Becklin, E. E., Gatley, I., and Werner, M. W. 1980, *Ap. J.*, 241, 709.

*Format differs from standard NASA publication If you have questions about a particular reference, please question the author(s) or the NASA contact point listed on the standard bibliography page

Israel, F. 1978, *Astr. Ap.*, 70, 769.

Ito, K., Matsumoto, T., and Uyama, K. 1977, *Nature*, 265, 515.

Krassner, J., Pipher, J. L., Savedoff, M. P., and Soifer, B. T. 1983, *A.J.*, 88, 972.

Leisawitz, D., and Bash, F. N. 1984, *Ap. J.*, in press.

Lester, D. F., Dinerstein, H. L., Werner, M. W., Watson, D. M., and Genzel, R. 1983, *Ap. J*, 271, 618.

_____. 1985, in preparation.

Lockman, F. J. 1976, *Ap. J.*, 209, 429.

Low, F. J., Kurtz, R. F., Poteet, W. M., and Nishimura, T. 1977, *Ap. J. (Letters)*, 214, L115.

Mezger, P. G. 1978, *Astr. Ap.*, 70, 565.

Mezger, P. G., Pankonin, B., Schmid-Burkg, J., Thum, C., and Wink, J. 1979, *Astr. Ap.*, 80, L3.

Mezger, P. G. and Smith, L. F. 1975, in *IAU Symposium 75, Star Formation*, ed. T. de Jong, and A. Maeder (Dordrecht: Reidel), p.133.

Miller, G. E., and Scalo, J . M. , 1979, *Ap. J. Suppl.*, 41, 533.

Nishimura, T., Low, F. J. and Kurtz, R. F. 1980, *Ap. J. (Letters)*, 239, L101.

Olthof, H. 1974, *Astr. Ap.*, 33, 471.

Panagia, N. 1973, *A. J.*, 78, 929.

Pipher, J. L., Grasdalen, G. L., and Soifer, B. T. 1974, *Ap. J.*, 193, 283.

Rodríguez, L. F., and Chaisson, E. J. 1978 *Ap. J.*, 221, 816.

Rubin, R. H. 1968, *Ap. J.*, 154, 391.

Schraml, J., and Mezger, P. 1969, *Ap. J.*, 156, 269.

Shaver, P. A., Radhakrishnan, V., Anantharamaiah, K. R., Retallack, D. S., Wamstecker, W., and Danks, A. C. 1982, *Astr Ap.*, 106, 105.

Scoville, N. Z., and Solomon, P. M. 1975, *Ap. J.*, 201, 352.

Taylor, J. H. 1979, in *IAU Symposium 84, The Large Scale Characteristics of the Galaxy*, ed. W. B. Burton (Dordrecht: Reidel), p. 119.

Thronson, H. A. Jr., and Harper, D. A. 1979, *Ap J.*, 230, 133.

Turner, B. E. 1979, *Astr. Ap. Suppl.*, 37, 1.

Turner, B. E., Balick, B., Cudaback, D. D., Heiles, C., and Boyle, R. J. 1974, *Ap J.*, 194, 279.

Wilson, T. L. 1972, *Astr. Ap.*, 19, 354.

Wynn-Williams, C. G., and Becklin, E. E. 1974, *Pub. A. S. P.*, 86, 5.

FIGURE CAPTIONS

Figure 1--- (a) upper left: 50μm and (b) lower left: 100μm maps of the G30.8 complex at an angular resolution of 50″; the beam is indicated in the upper left-hand corner. The designated source numbers are indicated in the 100μm map. The solid triangles (Δ) indicate the positions of the three prominent 100μm peaks. The asterisk (*) indicates the position of the unresolved 2μm source that may correspond to the ionizing star. The contour units for the 50μm map are 100, 300, 600, 900, 1200, 1500, and 1800 Jy per beam. The contour units for the 100μm map are 300, 600 900, 1200, 1500, 1800, and 2100 Jy per beam. (c) upper right: the color temperature map derived from the 50 and 100μm maps; the contours are 45, 55, 65, 75, and 85°K. (d) lower right: the integrated H_2CO equivalent width derived from the synthesis maps of Beiging, Wilson and Downes (1982). The much larger beam (2.5′ diameter) is indicated in the corner. The units are km-s^{-1} equivalent width. Comparing this map with the 50 and 100μm maps it can be seen that the H_2CO absorption is strongest over those far infrared components with the lowest apparent color temperature. As explained in the text, this is understandable in terms of large extinction optical depths.

Figure 2--- G30.8 is shown in a hybrid array VLA map at 6 cm. Contour levels are 2 , 3, 4, 5, 6, 7, 8, 9, 10, 15, 20, 25, 30 x 100 mJy per beam. The beam size and orientation is described in the text, and the symbols are as for Figure 1. This map is strikingly similar to the 100μm map in Figure 1b, showing that the stars which ionize the gas are probably responsible for heating the dust. The point source at the lower left may be a background source. The peripheral clouds of ionized gas mare seen to be arc-like, and are approximately centered on the near-IR source which is indicated by a plus sign (+), and which is also the position of peak dust temperature in this region. This object may be the source of excitation for most of the complex.

Figure 3 -- The far-infrared spectral distributions for various components of G30 8 are shown. The lower two curves correspond to the spectral flux per beam centered on the peaks G30.8N and S (sources 1 and 2 in that complex). Photometry for these sources was done in four bandpasses, which are indicated by horizontal lines at the bottom of the figure. A single error bar, which typifies the observational uncertainties in all measurements, is shown. Blackbody curves have been fitted through the 50 and 100μm points of these spectra, and these fits are indicated by the solid lines. The dashed lines are the actual spectral distributions, fitted by eye to all four wavelength points. The fact that the spectra are wider than blackbodies is indicative of nonisothermal dust distributions, but this excess width contributes negligibly to the total flux from each source. In the uppermost curve, a blackbody curve is fitted through the integrated 50 and 100μm fluxes for the entire nebula. This blackbody curve yields an approximate value for the total far-infrared flux form the G30.8 complex. Note that the two upper curves are normalized by scale factors in order to distinguish the curves on the graph.

Figure 4 --- (a) above: 50μm and (b) middle: 100μm maps of the G25.4 complex at an angular resolution of 50″, which is indicated in the upper left-hand corner. The plus signs (+) indicate the positions of the two peaks at 100μm. The contours for the 50μm map are 100, 200, 300, 500, 1000, 2000, 2500, 3000, and 3500 Jy per beam. The contours on the 100μm map are 300, 500, 1000, 1500, 2000, 2500, and 3000 Jy per beam. (c) bottom: color temperature map derived from the 50 and 100μm maps; contour units are 50, 60, 70, and 80°K.

Figure 5--- VLA map of G25.4 at 6 cm. Contour levels are 4, 5, 6, 7, 8, 9, 10, 15, 20, 30, 40, 50, 60, and 70 x 100 mJy per beam. The beam size and orientation is described in the text. This map was made mainly with a large antenna spacing, so low level extended emission is undersampled. G25.4SE and NW are the only sources visible.

Figure 6---A map of G25.4SE at [SIII] 9532Å made with a 30″ aperture. Contour units are 10^{-12} erg-cm^{-2}- s^{-1} in this aperture. The positions of peak flux at this wavelength is probably consistent with that of the radio continuum and far-infrared peak to within the errors of measurement.

Figure 7---H86α spectra of G25.4SE and NW are compared. Note the pronounced velocity shift (≈40 km-s^{-1}) between these two compact HII regions that are only 2.5′ apart in the sky. These spectra show that the two components, previously thought to be physically associated, are just coincidentally superimposed. The corresponding recombination line of helium is barely visible at V≈-80 km-s^{-1}.

Figure 8--- ^{13}CO (2-1) maps of G25.4 taken in a 1′ (FWHM) beam at MWO. Contours in °K antenna temperature are indicated separately for the two dominant velocity components. The molecular gas reflects the complicated velocity structure that is found from H86å in the ionized gas. The far-infrared centroids of G25.4SE and G25.4NW are indicated for reference.

Figure 9--- Same as for Figure 3 except for G25.4-0.2.

Figure 10--- 100 μm fluxes of W43 from different investigations are compared. The integrated fluxes are plotted as a function of effective beam size. The cited values, in order of decreasing beam size, are from Boissé *et. al* (1981), Olthof (1974), Low *et. al.* (1977), Hoffman, Frederick, and Emery (1971), and this paper.

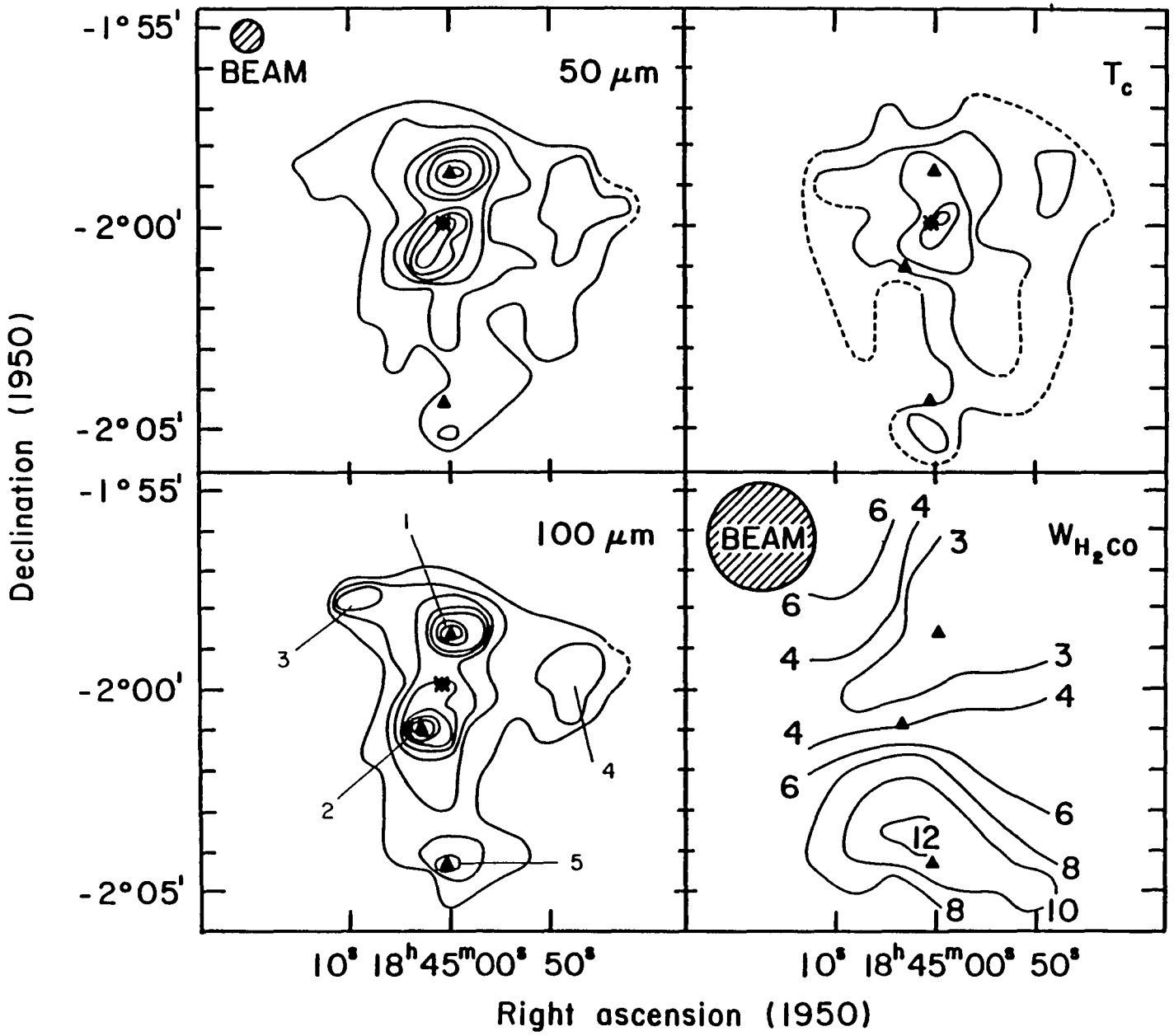
-1°55'
-2°00'
-2°05'
BEAM
50 μm
T_c
100 μm
BEAM
W_{H_2CO}
1
2
3
4
5
6
4
3
4
4
6
6
12
8
8
10
10s 18h45m00s 50s
10s 18h45m00s 50s
Declination (1950)
Right ascension (1950)

Fig. 1

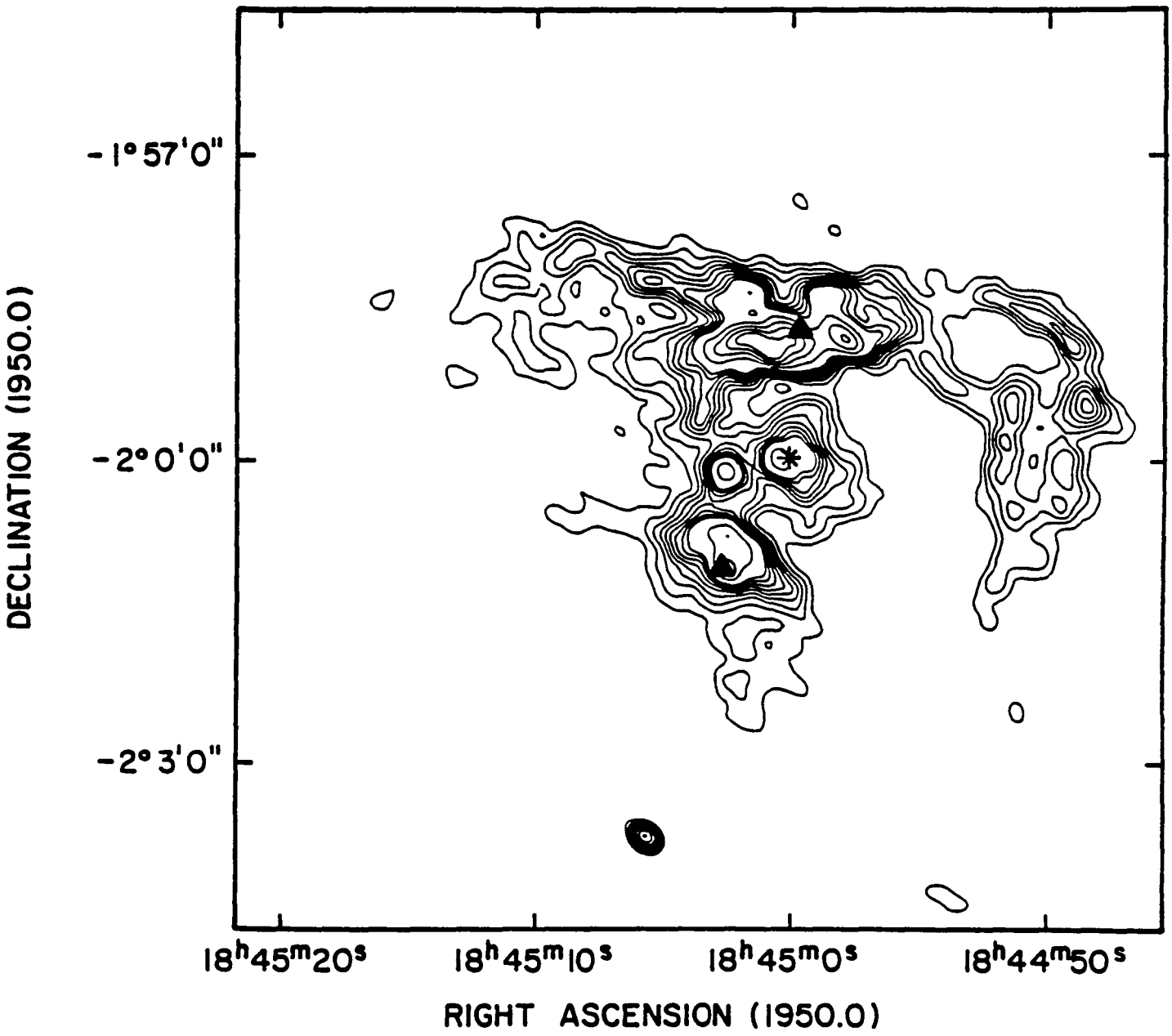
-1°57'0"
-2°0'0"
-2°3'0"
DECLINATION (1950.0)
18h45m20s
18h45m10s
18h45m0s
18h44m50s
RIGHT ASCENSION (1950.0)

Fig. 2

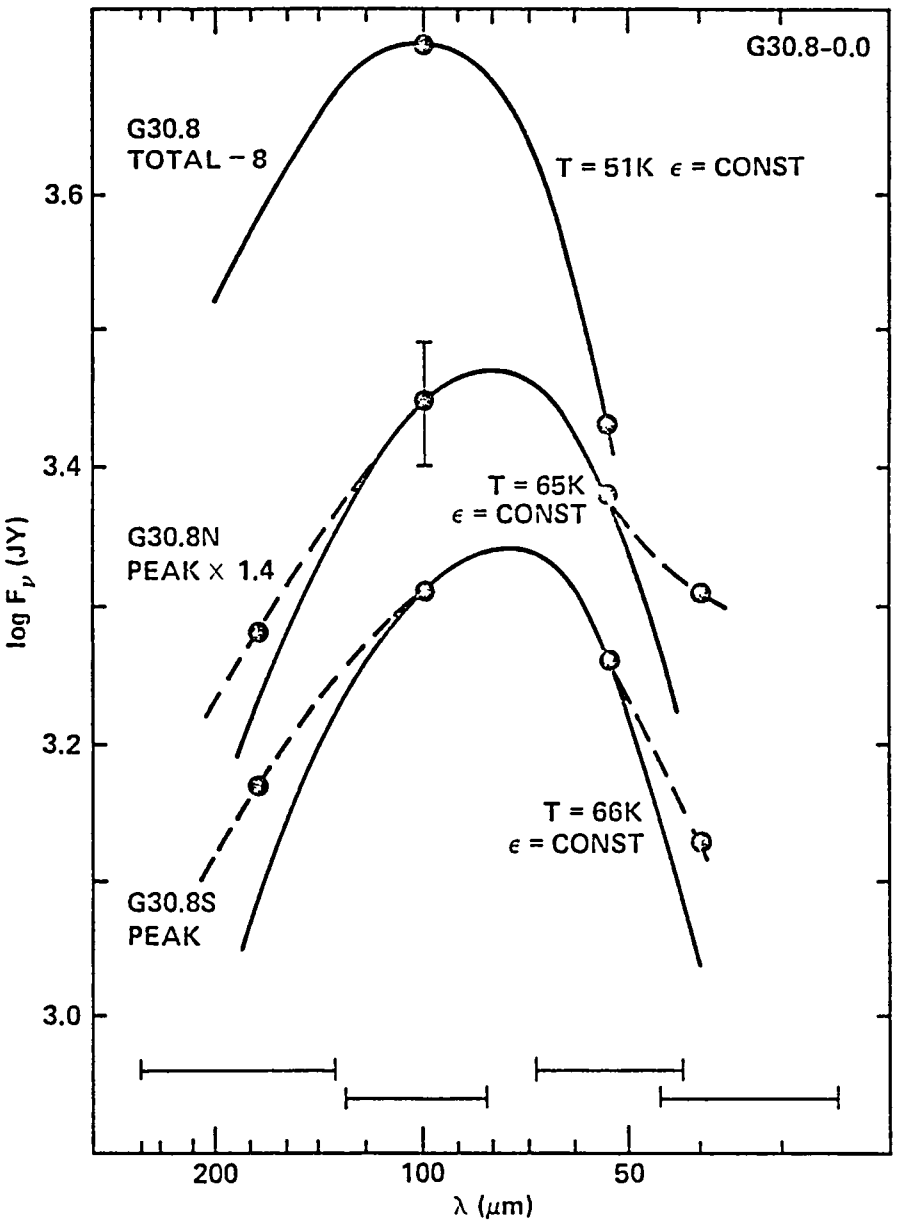
G30.8-0.0
G30.8
TOTAL − 8
T = 51K ϵ = CONST
T = 65K
ϵ = CONST
G30.8N
PEAK × 1.4
T = 66K
ϵ = CONST
G30.8S
PEAK
3.6
3.4
3.2
3.0
log F_ν (JY)
200
100
50
λ (μm)

Fig. 3

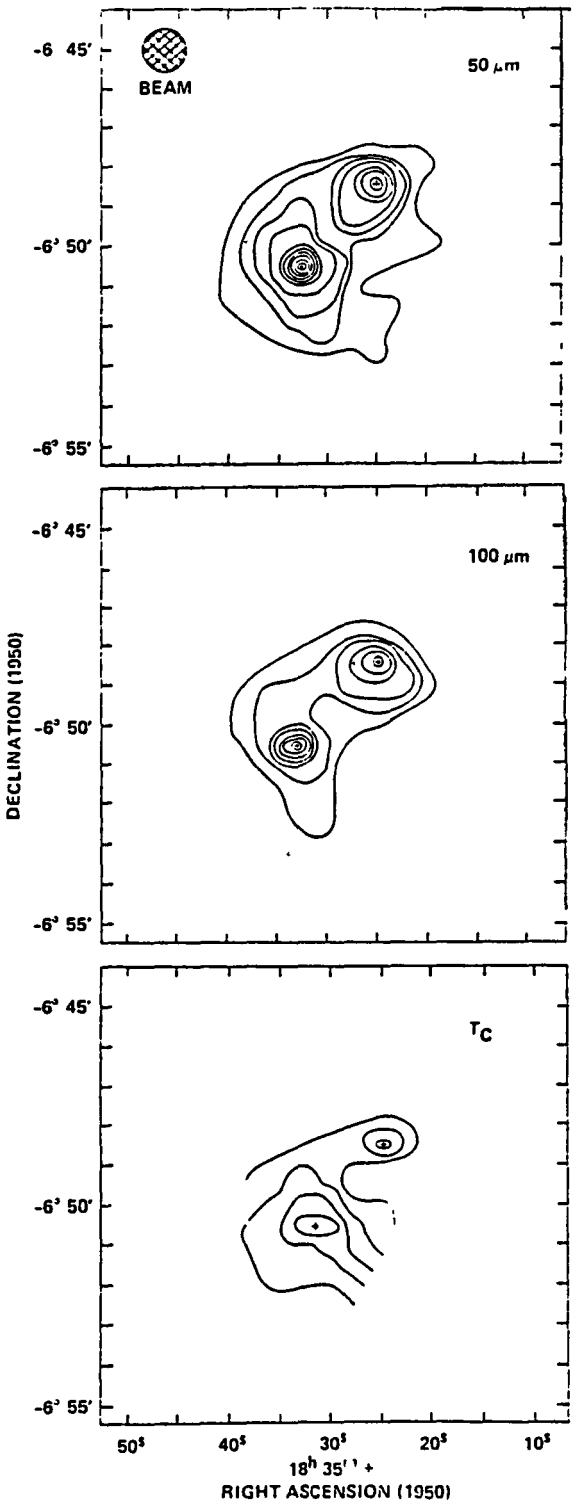
-6 45'
BEAM
50 μm
-6° 50'
-6° 55'
-6° 45'
100 μm
-6° 50'
-6° 55'
DECLINATION (1950)
-6° 45'
T_C
-6° 50'
-6° 55'
50^s
40^s
30^s
20^s
10^s
18^h 35' ' +
RIGHT ASCENSION (1950)

Fig. 4

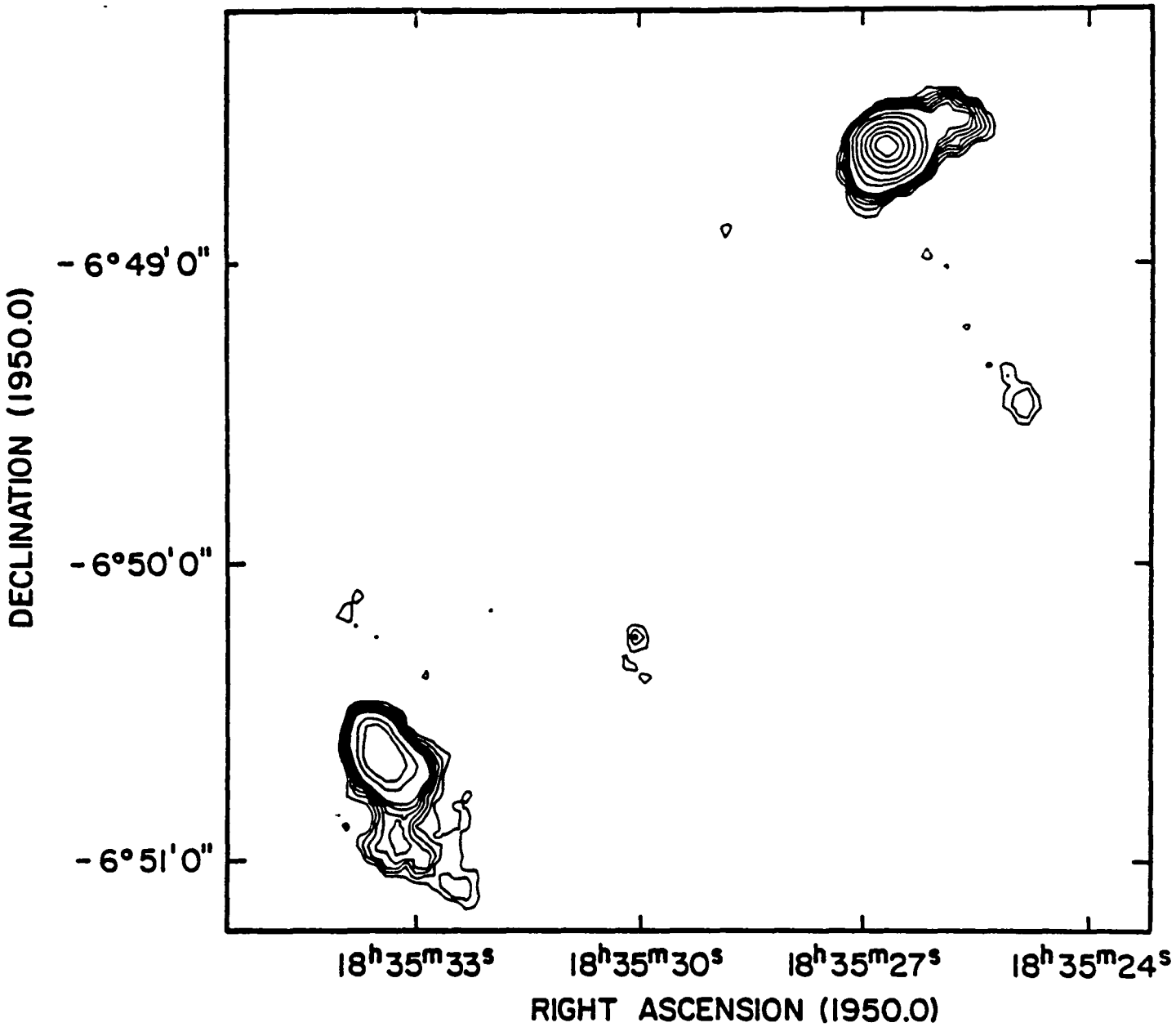
-6°49'0"
-6°50'0"
-6°51'0"
DECLINATION (1950.0)
18h35m33s
18h35m30s
18h35m27s
18h35m24s
RIGHT ASCENSION (1950.0)

Fig. 5

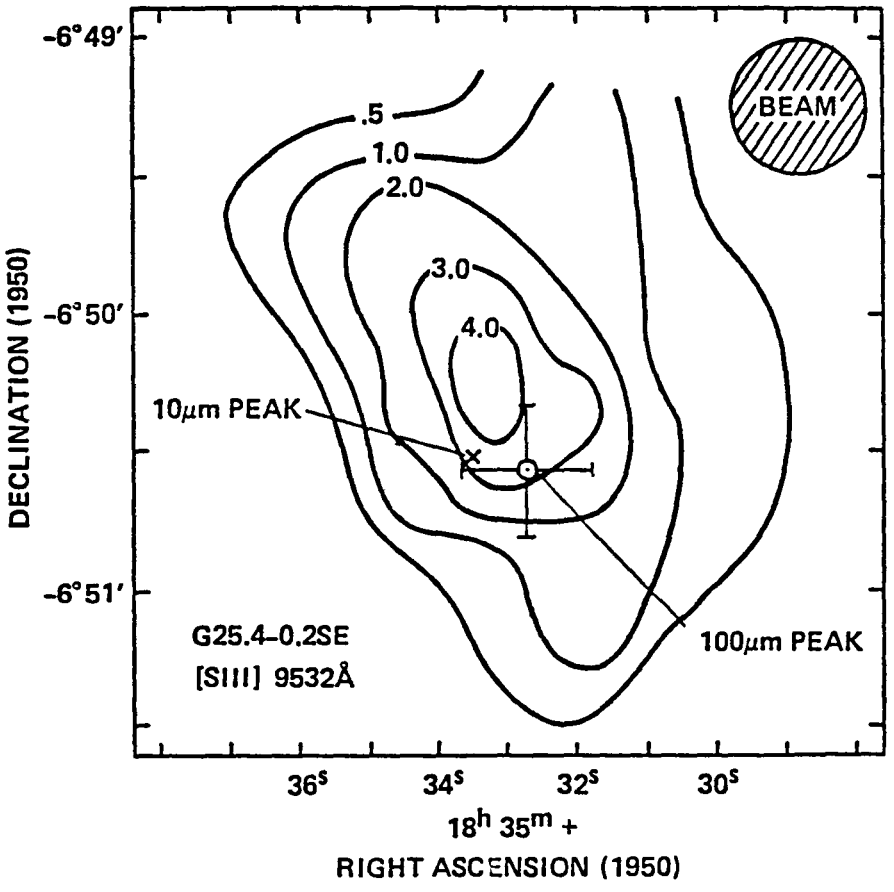
-6°49′
-6°50′
-6°51′
DECLINATION (1950)
.5
1.0
2.0
3.0
4.0
BEAM
10μm PEAK
100μm PEAK
G25.4-0.2SE
[SIII] 9532Å
36ˢ
34ˢ
32ˢ
30ˢ
18ʰ 35ᵐ +
RIGHT ASCENSION (1950)

Fig. 6

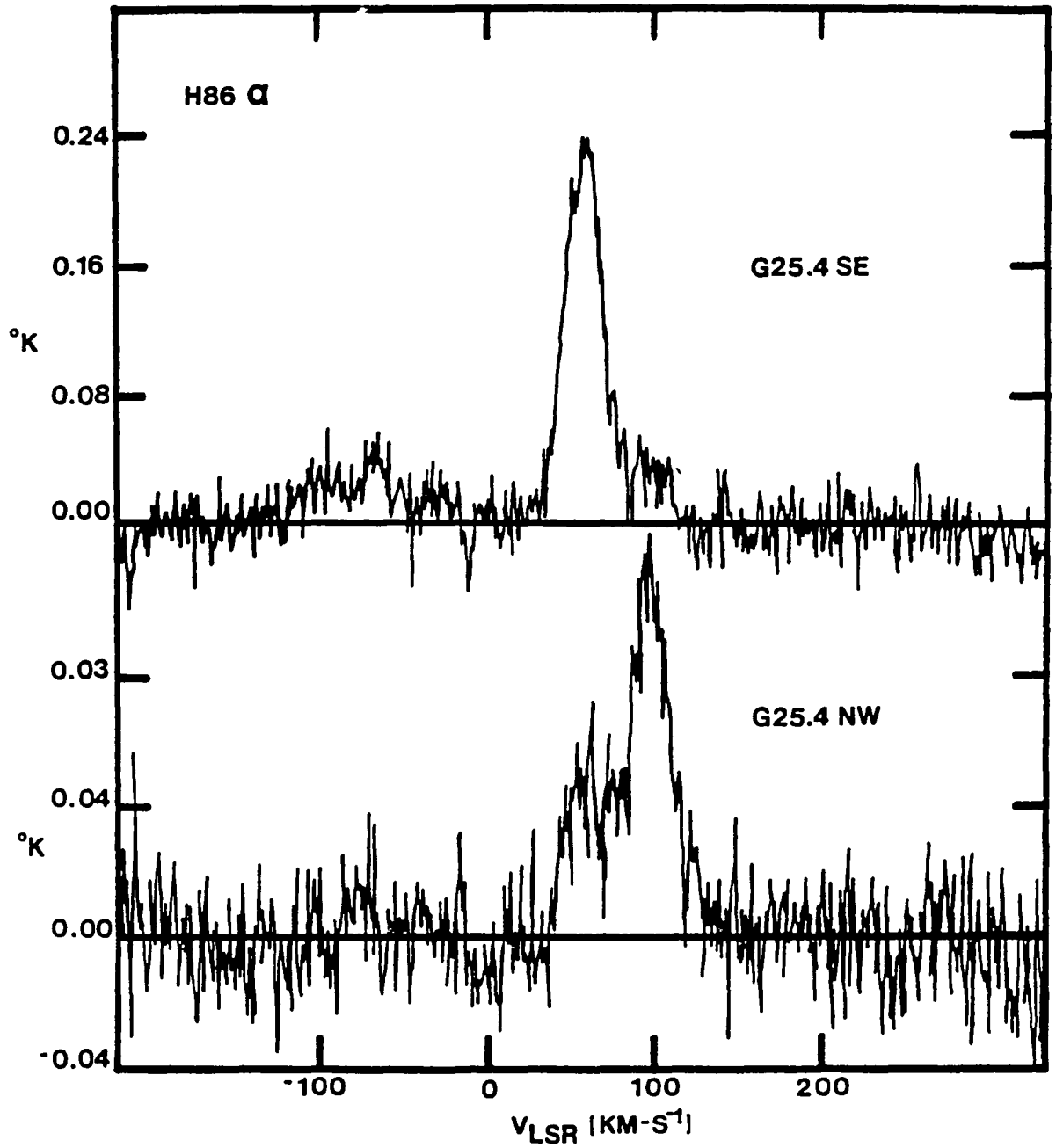
H86 α
G25.4 SE
G25.4 NW
°K
°K
0.24
0.16
0.08
0.00
0.03
0.04
0.00
-0.04
-100
0
100
200
V_LSR [KM-S^-1]

Fig. 7

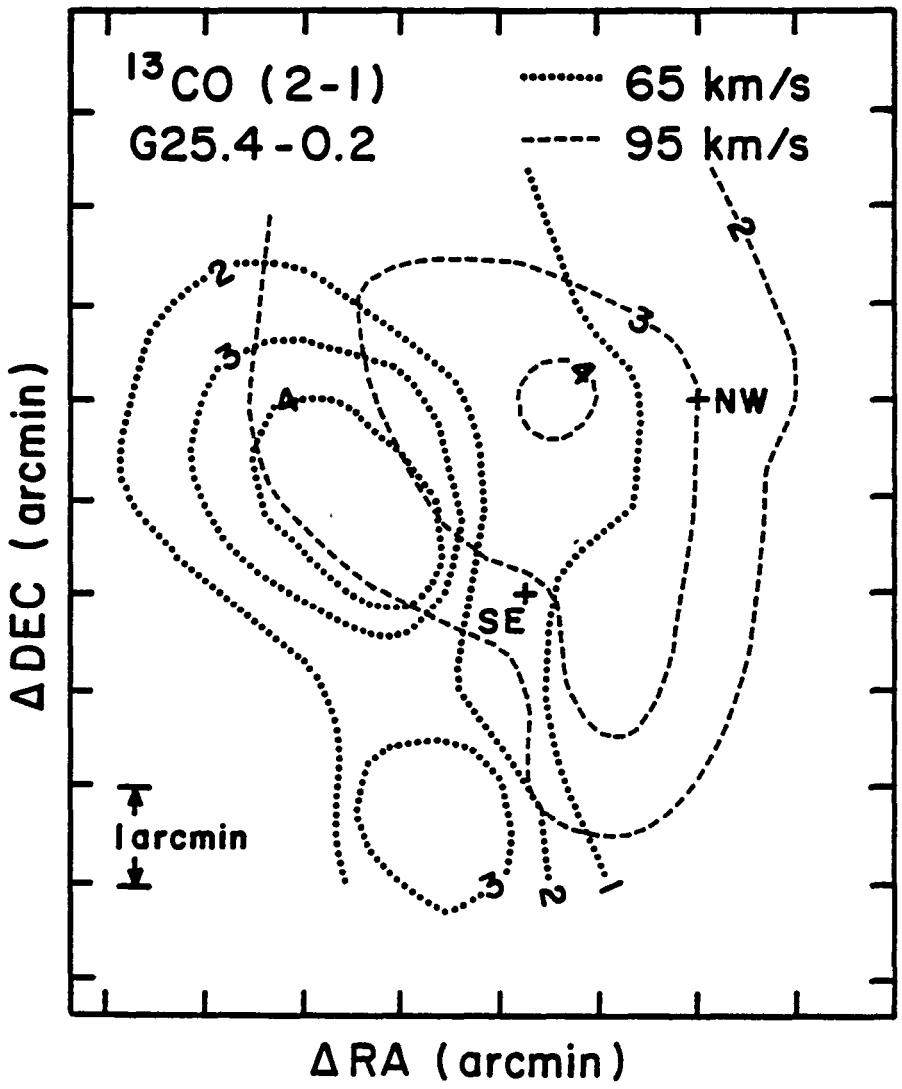
^{13}CO (2-1)
G25.4-0.2
65 km/s
95 km/s
NW
SE
1arcmin
ΔDEC (arcmin)
ΔRA (arcmin)

Fig. 8

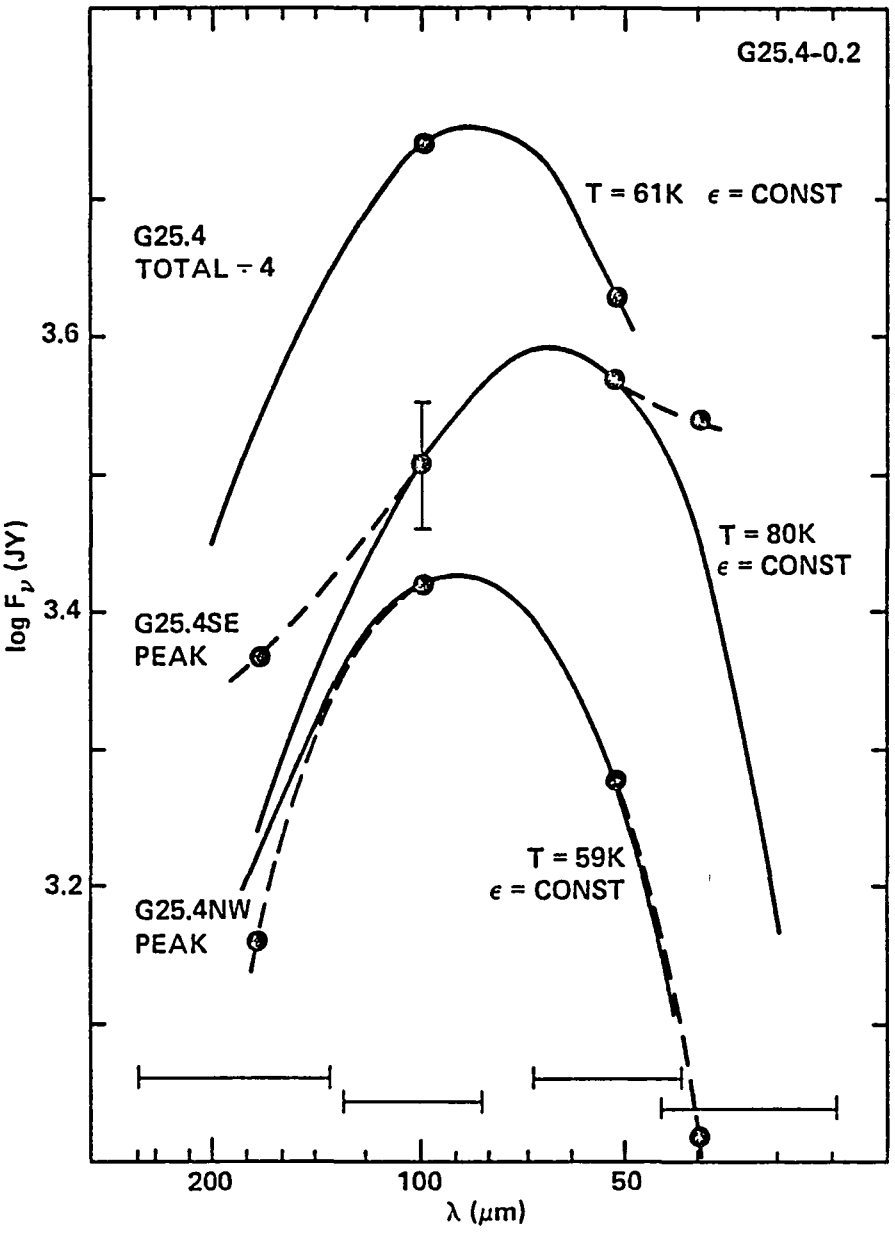
G25.4-0.2
T = 61K ϵ = CONST
G25.4
TOTAL ÷ 4
T = 80K
ϵ = CONST
G25.4SE
PEAK
T = 59K
ϵ = CONST
G25.4NW
PEAK
3.6
3.4
3.2
log F$_\nu$ (JY)
200
100
50
λ (μm)

Fig. 9

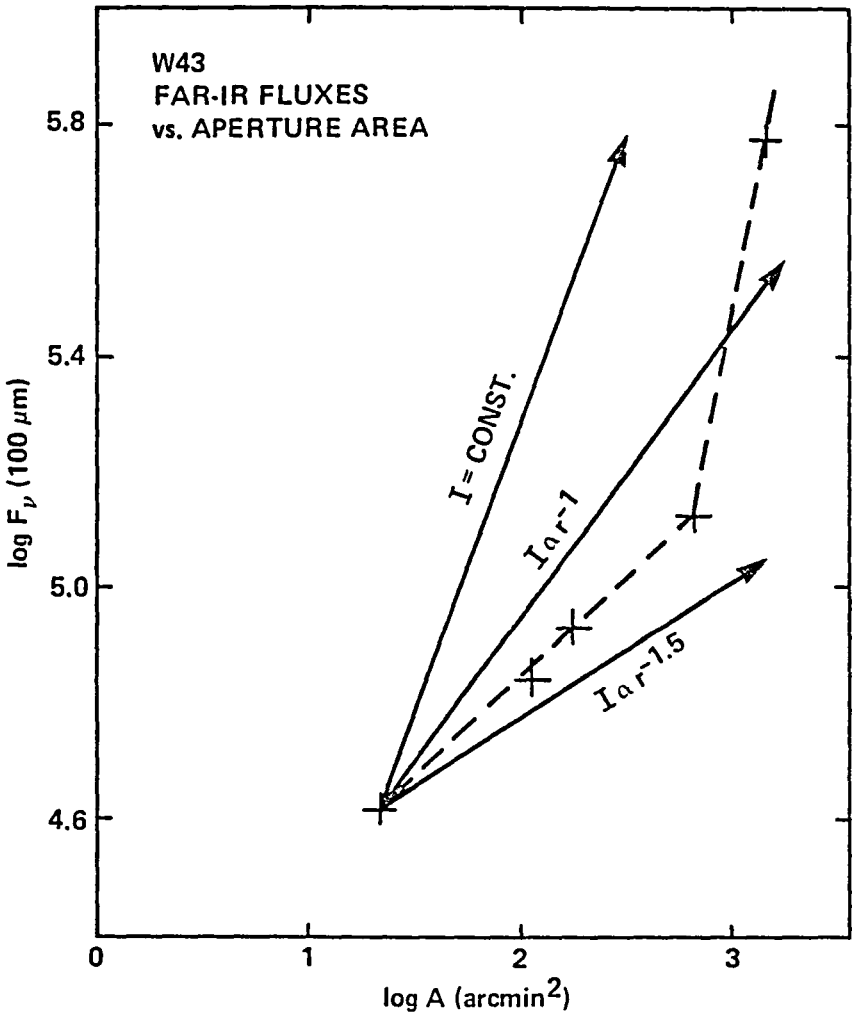
W43
FAR-IR FLUXES
vs. APERTURE AREA
5.8
5.4
5.0
4.6
log F_ν (100 μm)
0
1
2
3
log A (arcmin^2)
I= CONST.
I∝r^{-1}
I∝r$^{-1.5}$

Fig. 10

AUTHORS ADDRESSES:

R. L. BROWN
National Radio Astronomy Observatory
Edgemont Road
Charlottesville, VA 22901

H. L. DINERSTEIN
N. J. EVANS II
P. M. HARVEY
D. F. LESTER
Department of Astronomy
University of Texas at Austin
Austin TX 78712

M. W. WERNER
Astrophysical Experiments Branch MS245-6
NASA Ames Research Center
Moffett Field CA 94035

1 Report No	2 Government Accession No	3 Recipient's Catalog No
NASA TM-88184		

4 Title and Subtitle	5 Report Date
STAR FORMATION IN THE INNER GALAXY: A FAR-INFRARED AND RADIO STUDY OF TWO H II REGIONS	December 1985
	6 Performing Organization Code

7 Author(s)	8 Performing Organization Report No
D. F. Lester*,‡H. L. Dinerstein*, M. W. Werner†, P. M. Harvey‡, N. J. Evans II†, and R. L. Brown§	86008
	10 Work Unit No
9 Performing Organization Name and Address *University of Texas at Austin, Austin, TX 78712 †Ames Research Center, Moffett Field, CA 94035 ‡University of Texas at Austin, Austin, TX 78712 §National Radio Astronomy Observatory, Charlottesville, VA 22901	11 Contract or Grant No
	13 Type of Report and Period Covered Technical Memorandum
12 Sponsoring Agency Name and Address National Aeronautics and Space Administration Washington, DC 20546	14 Sponsoring Agency Code 352-02-03

15 Supplementary Notes

Preprint Series #38. Supported by NASA grants.

Point of Contact: L. C. Haughney, Ames Research Center, MS 211-12, Moffett Field, CA 94035, (415) 694-5339 or FTS 464-5339

16 Abstract

Far-infrared and radio continuum maps have been made of the central 6' of the inner-galaxy H II regions G30.8-0.0 (in the W43 complex) and G25.4-0.2, along with radio and molecular line measurements at selected positions. The purpose of this study is an effort to understand star formation in the "molecular ring" at 5 kpc in galactic radius. Measurements at several far infrared wavelengths allow the dust temperature structures and total far infrared fluxes to be determined. Comparison of the radio and infrared maps shows a close relationship between the ionized gas and the infrared-emitting material. There is evidence that parts of G30.8 are substantially affected by extinction, even at far-infrared wavelengths.

For G25.4-0.2, our radio recombination line and CO line data allow us to resolve the distance ambiguity for this source. The large distance previously ascribed to the entire complex is found to apply to only one of the two main components. The confusion in distance determination is found to result from an extraordinary near-superposition of two bright H II regions. Using our revised distances of 4.3 kpc for G25.4SE and 12 kpc for G25.4NW, we find that the latter, which is apparently the fainter of the two sources, is actually the more luminous. Though it is not seen on the Palomar Sky Survey, G25.4SE is easily visible in the 9532Å line of [S III] and was mapped in this line.

The ratio of total luminosity to ionizing luminosity is very similar to that of H II regions in the solar circle. Assuming a coeval population of ionizing stars, a normal initial mass function is indicated.

17 Key Words (Suggested by Author(s))	18 Distribution Statement
Far-infrared: two H II regions Star formation: inner galaxy	Unlimited Subject category - 89

19 Security Classif (of this report)	20 Security Classif (of this page)	21 No of Pages	22 Price*
Unclassified	Unclassified	41	A03

*For sale by the National Technical Information Service, Springfield, Virginia 22161

End of Document